

Laminin 111-based defined culture promoting self-renewing human pluripotent stem cells with properties of the early post-implantation epiblast

Michal Gropp,¹ Ithai Waldhorn,¹ Yaniv Gil,¹ Debora Steiner,¹ Tikva Tako Turetsky,¹ Yoav Smith,² Ofra Sabag,³ Tal Falick-Michaeli,⁴ Sharona Even Ram,¹ and Benjamin E. Reubinoff^{1,5,*}

¹The Hadassah Stem Cell Research Center, Goldyne Savad Institute of Gene Therapy, Hadassah-Hebrew University Medical Center, 91120 Jerusalem, Israel

²The Faculty of Medicine, Hebrew University of Jerusalem, Jerusalem, Israel

³Department of Developmental Biology and Cancer Research, Faculty of Medicine, Hebrew University of Jerusalem, Israel

⁴Rubin Chair in Medical Science, Department of Developmental Biology & Cancer Research, IMRIC, Faculty of Medicine, Hebrew University of Jerusalem, Jerusalem, Israel

⁵Department of Obstetrics and Gynecology, Hadassah-Hebrew University Medical Center, 91120 Jerusalem, Israel

*Correspondence: benr@hadassah.org.il

<https://doi.org/10.1016/j.stemcr.2022.10.010>

SUMMARY

In the mammalian embryo, a formative pluripotent phase is proposed to exist at the early post-implantation period, during the transition from the pre-implantation naive—to the post-implantation primed—epiblast. By recapitulating a laminin component of the extracellular matrix niche during embryonic formative transition, and defined culture conditions, we generated cultures highly enriched for self-renewing human pluripotent stem cells (hPSCs), exhibiting properties of early post-implantation epiblast cells. These hPSCs display post-implantation-epiblast gene expression profiles. FGF and TGF- β signaling maintain their self-renewal for multiple passages. They have inactive canonical Wnt signaling, do not express primitive streak markers, and are competent to initiate differentiation toward germline and somatic fates. hPSCs exhibiting early post-implantation epiblast properties may shed light on human embryonic PSCs development and may serve for initiating somatic and germ cell specification.

INTRODUCTION

Two distinct phases of pluripotency have been defined in the mouse embryo: a "naive" phase that exists at the pre-implantation inner cell mass (ICM), and a "primed" phase that exists at the post-implantation epiblast (Nichols and Smith, 2009). Naive mouse embryonic stem cells (ESCs) derived from ICM cells (Evans and Kaufman, 1981), and primed mouse epiblast stem cells (mEpiSCs) derived from post-implantation epiblast cells (Brons et al., 2007; Tesar et al., 2007), exhibit distinct transcriptomes, epigenomes, and growth factor requirements.

Human ESCs (hESCs) are derived from the ICM (Reubinoff et al., 2000; Thomson et al., 1998). Surprisingly, hESCs share properties with mEpiSCs and early post-implantation primate epiblasts (Nakamura et al., 2016), suggesting that they progress in culture to a more primed pluripotency state (Nichols and Smith, 2009). Culture conditions promoting naive hPSCs were developed by several groups (Gafni et al., 2013; Takashima et al., 2014; Theunissen et al., 2014).

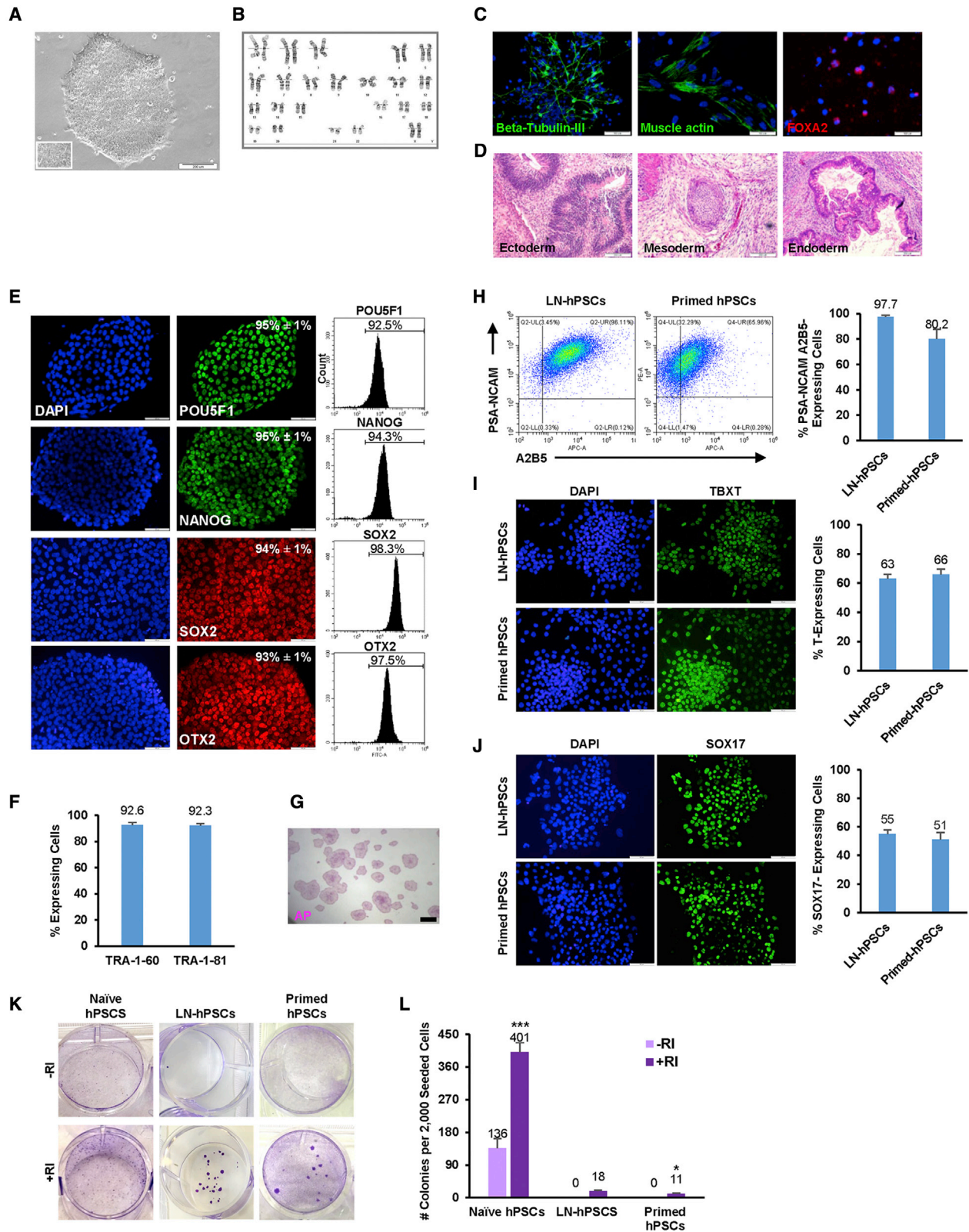
Lately, it was hypothesized that pluripotent cells progress from the naive to the primed phase through an intermediate "formative" phase existing in the early post-implantation epiblast (Smith, 2017). The formative phase may be represented in the mouse system by mouse epiblast-like cells (mEpiLCs), which exhibit a transcriptome resembling the early post-implantation epiblast, and can differentiate into primordial germ cells (PGCs). Notably, primed mEpiSCs lose the potential to generate PGCs (Hayashi et al., 2011).

Several criteria were suggested to define the human formative pluripotency phase, including a transcriptome characteristic of the early post-implantation epiblast, lack of lineage-specific marker expression, and competence for somatic and germline lineage specification (Pera and Rosant, 2021). Recently, several groups have reported on hPSCs exhibiting naive-to-primed intermediate characteristics (Cornacchia et al., 2019; Kinoshita et al., 2021; Lau et al., 2020; Rostovskaya et al., 2019; Yu et al., 2021).

Here, we sought to develop cultures highly enriched for self-renewing hPSCs, capturing the formative pluripotency phase *in vitro*. Laminin-111 (LN111) is one of the major extracellular matrix (ECM) proteins expressed in the basement membranes of mouse embryos already at the pre-implantation stage (Li et al., 2003). Expression of genes encoding LN111 subunits was similarly observed in human ICM and pre-implantation epiblast cells (Stirparo et al., 2018). It was suggested that LN111 attaches to outer ICM cells, promoting ICM polarization and epiblast formation (Li et al., 2003). We therefore hypothesized that an LN111-based hPSC culture system may confer a pluripotency state resembling the early post-implantation epiblast.

Our results demonstrate that hPSCs cultured on LN111 in defined conditions generate cultures highly enriched for genetically stable, self-renewing hPSCs exhibiting properties of the early-post implantation epiblast. They display a transcriptome profile similar to the post-implantation epiblast, and do not express primitive streak (PS) markers. FGF/TGF- β -mediated signaling is required for their self-renewal. While





(legend on next page)



the canonical Wnt signaling is inactive in these cells, they respond to Wnt stimulation by activation of PS markers. Finally, we show that hPSCs cultured on LN111 are competent to initiate PGC specification. These results suggest that hPSCs cultured on LN111 in defined conditions may represent an early post-implantation epiblast-like pluripotency phase.

RESULTS

Development of an LN111-based defined system promoting prolonged self-renewal of genetically stable hPSCs, retaining their pluripotent potential

In our culture system, we used LN111 as the ECM component at relatively high concentrations, enabling its polymerization, which is thought to initiate the basement membrane scaffold formation (Miner et al., 2004). To further promote the early post-implantation epiblast state, we cultured the hPSCs in a chemically defined serum-free medium containing N2/B27 and supplemented with FGF2. A similar medium composition was shown to induce and transiently maintain mEpiLCs in culture (Hayashi et al., 2011).

In our study, we characterized the properties of hPSCs cultured in this system (LN-hPSCs), and compared them with conventional/primed hPSCs cultured on mouse embryonic fibroblasts in KSR-containing medium, and 5iLA naive hPSCs (Theunissen et al., 2014).

LN-hPSCs (HES-1 cell line) formed homogeneous monolayer colonies comprised of tightly packed cells with high nucleus to cytoplasm ratios, and prominent nucleoli (Figure 1A). HES-1 cells could be propagated under these culture conditions for prolonged periods while maintaining a normal karyotype (passage 15), the expression of pluripotent

markers, and their pluripotent potential *in vitro* and *in vivo* (analyzed at passages 3–10; Figures 1B–1E and 1H–1J). Immunofluorescence staining and FACS analyses showed that the majority of LN-hPSCs uniformly expressed the key pluripotency regulators, as well as OTX2, a transcription factor (TF) associated with the mouse formative phase (Boroviak et al., 2015; Buecker et al., 2014) (Figure 1E). FACS analysis showed that over 90% of the cells expressed TRA-1-60 and TRA-1-81 cell-surface antigens (Figure 1F), and they displayed alkaline phosphatase activity (Figure 1G). We evaluated the competence of LN-, compared with primed hPSCs, to initiate differentiation *in vitro* into the three germ layers, using directed differentiation protocols. FACS and immunostaining analyses for the expression of early markers of neuroectoderm (PSA-NCAM and A2B5), mesoderm (TBXT), and endoderm (SOX17), revealed that LN-hPSCs exhibited enhanced neuroectodermal, and similar mesodermal and endodermal differentiation efficiencies compared with primed hPSCs (Figures 1H–1J). The cloning efficiency of LN-hPSCs in the presence of ROCK inhibitor was significantly lower than naive hPSCs, and higher than primed hPSCs (Figures 1K and 1L). Extended undifferentiated self-renewal under LN conditions was confirmed for an additional two hPSC lines (Figure S1).

Taken together, these results suggested that the LN111-based defined culture system promoted relative homogeneous cultures of self-renewing hPSCs.

The gene expression profile of LN-hPSCs resembles a post-implantation pluripotency state

We first analyzed the gene expression profiles of hPSC lines HES-1, HADC100, and HADC102 cultured on LN111 using the Human Stem Cell Pluripotency Gene Expression Array.

Figure 1. Laminin111-based defined culture conditions support prolonged self-renewal of genetically stable hPSCs, retaining their pluripotent potential

(A) Phase-contrast image of HES-1-LN hPSC colony with a magnified section. Scale bar, 200 μ m.

(B) Karyotype analysis of HES-1-LN-hPSCs cultured for 10 passages.

(C) Immunostaining of HES-1-LN-hPSCs differentiated *in vitro* into ectodermal (β -tubulin-III), mesodermal (muscle actin), and endodermal (FOXA2) cells.

(D) Histological analysis of teratomas generated from HES-1-LN-hPSCs. Scale bars, 200 μ m.

(E) Immunostaining and FACS analyses of POU5F1, NANOG, SOX2, and OTX2 in HES-1-LN-hPSCs. Immunostaining- POU5F1, SOX2, OTX2 (n = 3), NANOG (n = 5); FACS- POU5F1, NANOG (n = 5), SOX2, OTX2 (n = 4).

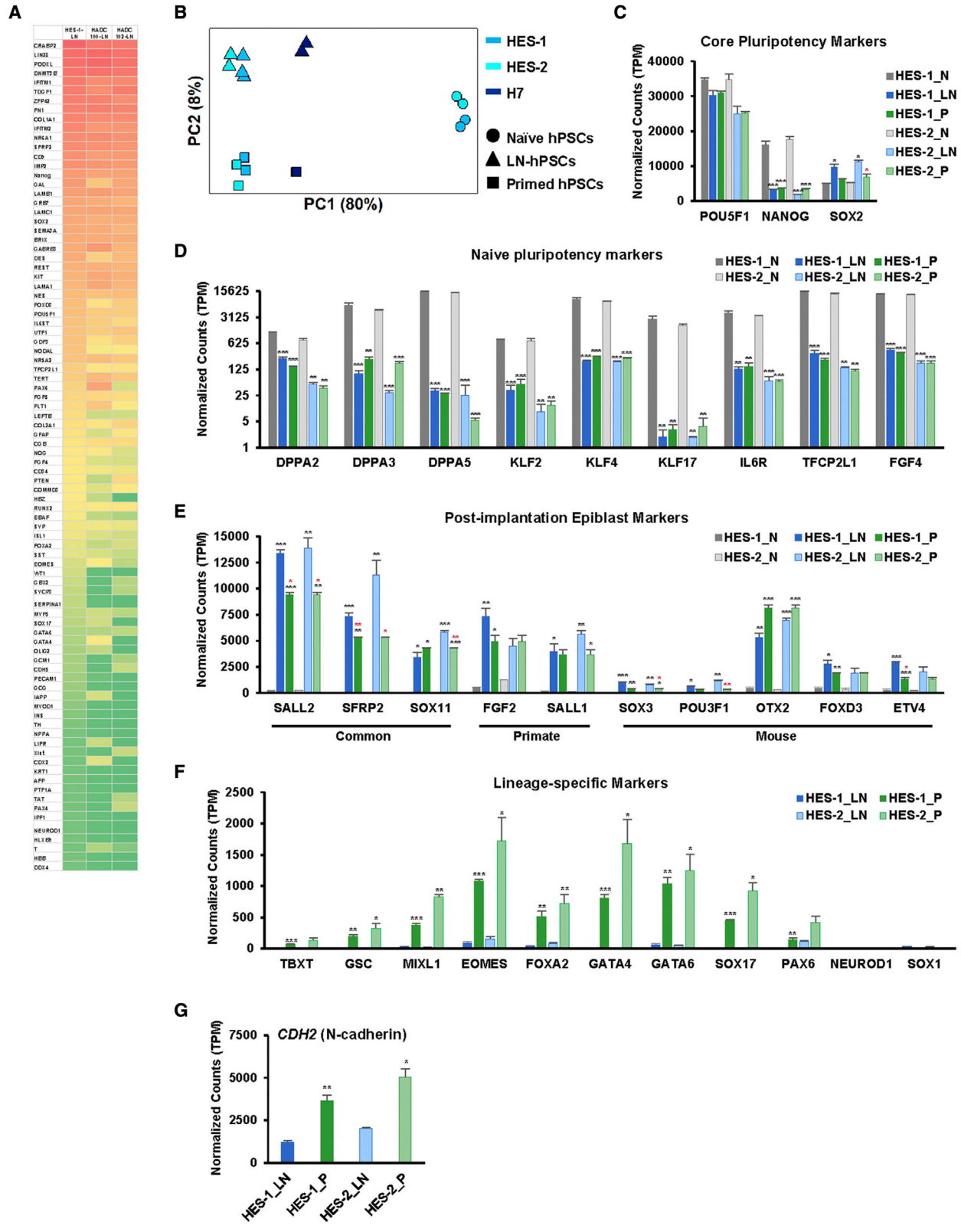
(F) FACS analysis of the expression of TRA-1-60 (n = 10) and TRA-1-81 (n = 7) in HES-1-LN-hPSCs.

(G) Image of alkaline phosphatase expression in HES-1-LN-hPSC colonies. Scale bar, 1 mm.

(H–J) FACS and immunostaining analyses of PSA-NCAM and A2B5 at day 7 of neural induction (H), TBXT at day 3 of mesodermal induction (I), and SOX17 at day10 of endodermal induction (J), in differentiated HES-1-LN- and primed hPSCs. n = 3 for all experiments.

(K and L) Images (K) and quantification (L) of crystal violet staining of colonies formed from single-cell suspensions of HES-1 hPSCs cultured under naive, LN, and primed conditions, \pm Y27632 (RI).

Data are mean \pm SEM of (n) wells $-RI$ hPSCs n \geq 4, $+RI$ -naive hPSCs n \geq 7. p values were calculated using two-tailed Student's t test for naive and primed hPSCs versus LN-hPSCs, seeded with RI. *p < 0.05, ***p < 0.001. (E, F, and H–J) Data are mean \pm SEM of (n) independent experiments. (C, E, and I–J) Nuclei are counterstained with DAPI (blue). Scale bars, 100 μ m.



(legend on next page)



All three hPSC lines expressed similarly high levels of pluripotency-associated genes, while lineage-specific genes were minimally expressed (Figure 2A; Table S1). These results confirmed that LN-hPSCs displayed gene expression profiles consistent with undifferentiated hPSCs.

To analyze the global transcriptome of LN-hPSCs in comparison with primed and naive hPSCs, we performed RNA sequencing (RNA-seq) of three hPSC lines HES-1, HES-2, and H7 cultured under LN, primed, and naive conditions (Table S2). Principal-component analysis (PCA) of the various hPSC samples discriminated the naive hPSCs from the other hPSCs on the PC1 axis, while LN-hPSCs and primed hPSCs were separated on PC2 (Figure 2B). Differential gene expression analysis (\log_2 fold change > 1, adjusted p value < 0.01) between LN- and primed hPSCs, identified 316 differentially expressed genes (DEGs) that were upregulated, and 543 DEGs that were downregulated, in LN-hPSCs relative to primed hPSCs. Pathway enrichment analysis showed that DEGs downregulated in LN-hPSCs were enriched for "embryonic morphogenesis," "gastrulation," "mesodermal commitment," and "epithelial cell differentiation." DEGs upregulated in LN-hPSCs were enriched among others for pathways regulating "synaptic transmission," "system process," and "cell-cell adhesion" (Figures S2A and S2B; Table S3).

We analyzed the expression of selected core, naive, and post-implantation pluripotency-associated genes in LN-hPSCs compared with primed and naive hPSCs. Of the three core pluripotency TFs, *POU5F1* was expressed at similar levels in LN-, naive, and primed hPSCs. Naive hPSCs expressed significantly higher levels of *NANOG* compared with LN- and primed hPSCs, while *SOX2* was expressed at higher levels in LN-hPSCs compared with naive and primed hPSCs (Figures 2C and S2C). Naive pluripotency markers were expressed at significantly lower levels in LN- and primed hPSCs compared with naive hPSCs (Figure 2D). qRT-PCR analysis confirmed significant lower expression levels of several naive pluripotency markers in LN- relative to 5iLFA-naive hPSCs (Figure S2D). We

further analyzed post-implantation markers characteristic to the primate early post-implantation epiblast (*FGF2* and *SALL1*), the early post-implantation mouse epiblast (*SOX3*, *POU3F1*, *OTX2*, *FOXD3*, and *ETV4*), and markers common to both primate and mouse early post-implantation epiblast (*SALL2*, *SFRP2*, and *SOX11*) (Boroviak et al., 2015; Nakamura et al., 2016). The selected markers were expressed at significantly higher levels in LN- and primed hPSCs compared with naive hPSCs. Notably, *SALL2* and *SFRP2* were expressed at significantly higher levels in LN- compared with primed hPSCs (Figure 2E). Single-cell RNA-seq (scRNA-seq) and qRT-PCR analyses confirmed significantly higher expression levels of *SALL2* and *SFRP2*, in LN- compared with primed hPSCs (Figures S2E and S2F).

RNA-seq and qRT-PCR analyses of the expression of selected lineage-specific markers showed that LN-hPSCs minimally expressed early PS markers, compared with primed hPSCs, which showed significantly higher expression of these markers (Figures 2F and S2G). In addition, the expression of *CDH2* encoding N-cadherin, which was shown to be upregulated in epiblast cells undergoing epithelial to mesenchymal transition during gastrulation (Gheldof and Berx, 2013), as well as in mouse EpiSCs compared with formative-like mPSCs (Wang et al., 2021), was significantly upregulated in primed compared with LN-hPSCs (Figure 2G).

To compare the transcriptome of LN-hPSCs with PSCs from human embryos, we performed PCA of LN-, naive, and primed hPSC RNA-seq data, and published scRNA-seq data of epiblast cells from days 6 and 7 of pre-implantation human embryos (Petropoulos et al., 2016; Stirparo et al., 2018), and days 6, 8, 10, and 12 epiblast cells from human embryos cultured *in vitro* (Zhou et al., 2019a). PC1 separated LN-, naive, and primed hPSCs from the embryonic epiblast cells. Embryonic epiblast cells were resolved by PC2, and plotted according to their developmental stage. In PC2, naive hPSCs aligned more closely to pre-implantation epiblast cells, while LN- and primed hPSCs aligned in proximity to post-implantation epiblast cells.

Figure 2. The gene expression profile of LN-hPSCs resembles a post-implantation pluripotency state

(A) Heatmap of the Human Stem Cell Pluripotency Gene Expression Array, of LN-hPSCs (HES-1, HADC100, and HADC102). Gene expression is presented as Delta-Ct value. HES-1 sample data is the average of two independent experiments.

(B) PCA plot of RNA-seq data of HES-1, HES-2, and H7 hPSCs cultured under LN and primed conditions, and HES-1 and HES-2 hPSCs cultured under naive conditions. PCA was computed using the top variable 3,800 genes.

(C–E) RNA-seq data of selected core pluripotency (C), naive pluripotency (D), and post-implantation epiblast (E) associated genes, in naive, LN and primed HES-1 and HES-2 hPSCs. p values depicted in black show the significant statistical differences between the naive samples and LN and primed samples. p values depicted in red show the significant statistical differences between the LN and primed samples.

(F–G) RNA-seq data of selected lineage-specific genes (F) and *CDH2* (G) in LN and primed HES-1 and HES-2 hPSCs.

LN, LN-hPSCs; P, primed hPSCs; N, naive hPSCs. p values were calculated using two-tailed Student's t test when two groups were compared, and ANOVA test when three groups were compared. *p < 0.05, **p < 0.01, ***p < 0.001. (C–G) Data are mean \pm SEM of two independent samples (except for HES-1-LN- three samples). LN-hPSC samples were at passage 3.

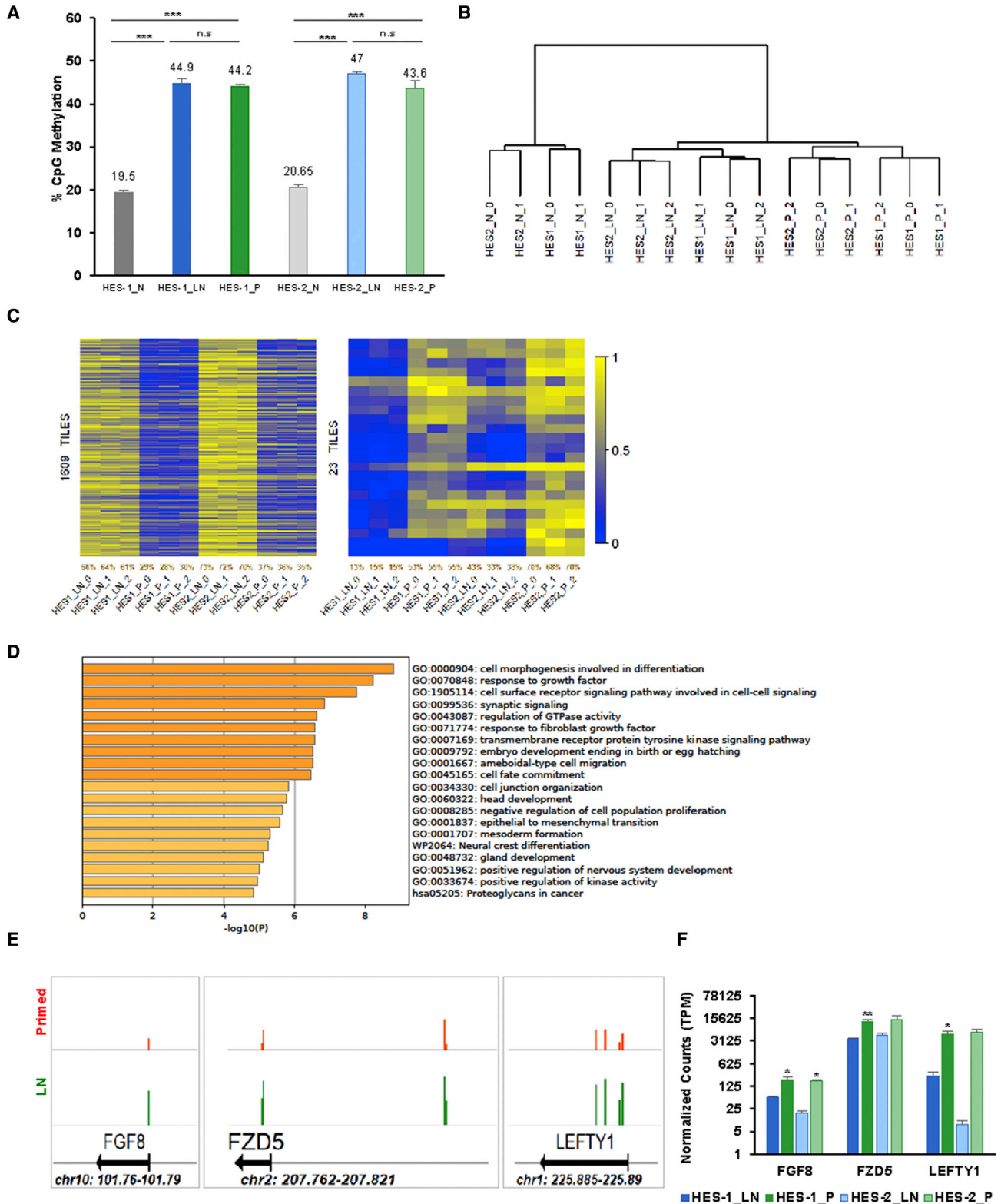


Figure 3. LN-hPSCs display a methylation profile characteristic of the post-implantation epiblast

(A) RRBS analysis showing average global CpG methylation levels of the autosomal chromosomes of naive, LN, and primed HES-1 and HES-2 hPSCs. Data are mean \pm SEM of (n) independent samples; naive hPSCs (n = 2), LN and primed hPSCs (n = 3).

(legend continued on next page)



In PC3, while LN- and primed hPSCs clustered adjacent to day 8 post-implantation epiblast cells, LN-hPSCs clustered more closely to day 7 pre-implantation embryonic epiblast cells compared with primed hPSCs (Figure S2H).

We further compared the transcriptome of LN-, naive, and primed hPSCs with published scRNA-seq data of cynomolgus monkey embryonic cells (ESCs) (Nakamura et al., 2016). PCA showed that PC1 separated pre- and post-implantation monkey PSCs. In PC1, naive hPSCs clustered between pre- and post-implantation monkey PSCs, while LN- and primed hPSCs clustered near the post-implantation epiblast and gastrulating cells. PC2 separated the post-implantation monkey cell populations according to the developmental progression of the epiblast. In this dimension, LN- and primed hPSCs were closely clustered, with the primed hPSCs distributed more toward gastrulating monkey cells (Figure S2I).

Taken together, the gene expression analyses suggested that the transcriptome of LN-hPSCs was distinct from the naive pre-implantation state and was consistent with a post-implantation state. The minimal expression of lineage-specific markers in LN-hPSCs suggested that they are related to the early post-implantation phase.

LN-hPSCs display a methylation profile resembling the post-implantation epiblast

Pre-implantation human embryos and naive hPSCs are marked by global hypomethylation, while primed hPSCs feature global hypermethylation (Takashima et al., 2014).

To evaluate the methylation status of LN-hPSCs, we performed reduced representation bisulfite sequencing (RRBS) of HES-1 and HES-2 hPSC lines cultured under LN, primed, and naive conditions. hPSCs cultured under naive conditions exhibited hypo-CpG methylation levels, whereas under LN and primed conditions they showed significantly increased and similar DNA methylation levels (Figure 3A). Unsupervised hierarchical clustering discriminated the naive hPSCs from LN- and primed hPSCs, whereas LN- and primed hPSCs clustered separately within the same subgroup (Figure 3B). While LN- and primed hPSCs exhibited similar global DNA methylation levels, we identified 1,609 DMRs that were hypermethylated, and 23 DMRs that were hypomethylated in LN- compared with

primed hPSCs (methylation difference >30%, adjusted p value ≤ 0.01) (Figure 3C; Table S4). The hypermethylated DMRs in LN-hPSCs (linked to 934 annotated genes) were enriched for pathways regulating differentiation and morphogenesis (Figure 3D). Interestingly, the hypermethylation of DMRs linked to *FGF8*, *LEFTY1*, and *FZD5* genes in LN- compared with primed hPSCs, was correlated with lower expression levels of these genes in LN- compared with primed hPSCs (Figures 3E and 3F). *FGF8* and *LEFTY1* were shown to be expressed during the developmental transition from pluripotency to gastrulation (Crossley and Martin, 1995; Tabibzadeh and Hemmati-Brivanlou, 2006).

The RRBS analysis showed that the methylation profile of LN-hPSCs is distinct from naive hPSCs, and resembles primed hPSCs, displaying methylation levels characteristic of the post-implantation epiblast.

The FGF and TGF- β /activin-dependent signaling pathways are required for the self-renewal of LN-hPSCs

The FGF-dependent MEK/ERK and PI3K/AKT signaling pathways, as well as the TGF- β /activin-dependent SMAD2/3 pathway, were shown to cooperatively maintain the self-renewal of the primed mEpiSCs (Tesar et al., 2007), primed hPSCs (James et al., 2005; Xu et al., 2005), as well as the transient proliferation of the formative-like mEpiLCs (Hayashi et al., 2011).

To analyze the signaling pathways that maintain the self-renewal of LN-hPSCs, we first assessed the expression of receptors and ligands of FGF signaling. RNA-seq analysis showed that LN-hPSCs expressed higher levels of *FGF2*, compared with *FGF4*. FGF receptor type 1 (*FGFR1*) was expressed at higher levels compared with the other three FGF receptors (Figure 4A). To further explore FGF signaling in LN-hPSCs, we cultured them for 2 days post-passaging in our basic medium, which is supplemented with FGF2, but does not include factors from the TGF- β superfamily, and for an additional 5 days under various modified conditions. Following FGF2 depletion, smaller hPSC colonies developed, however, with a typical undifferentiated morphology (Figure 4B). Moreover, TRA-1-60 as well as POU5F1 and NANOG expression levels were similar to cells

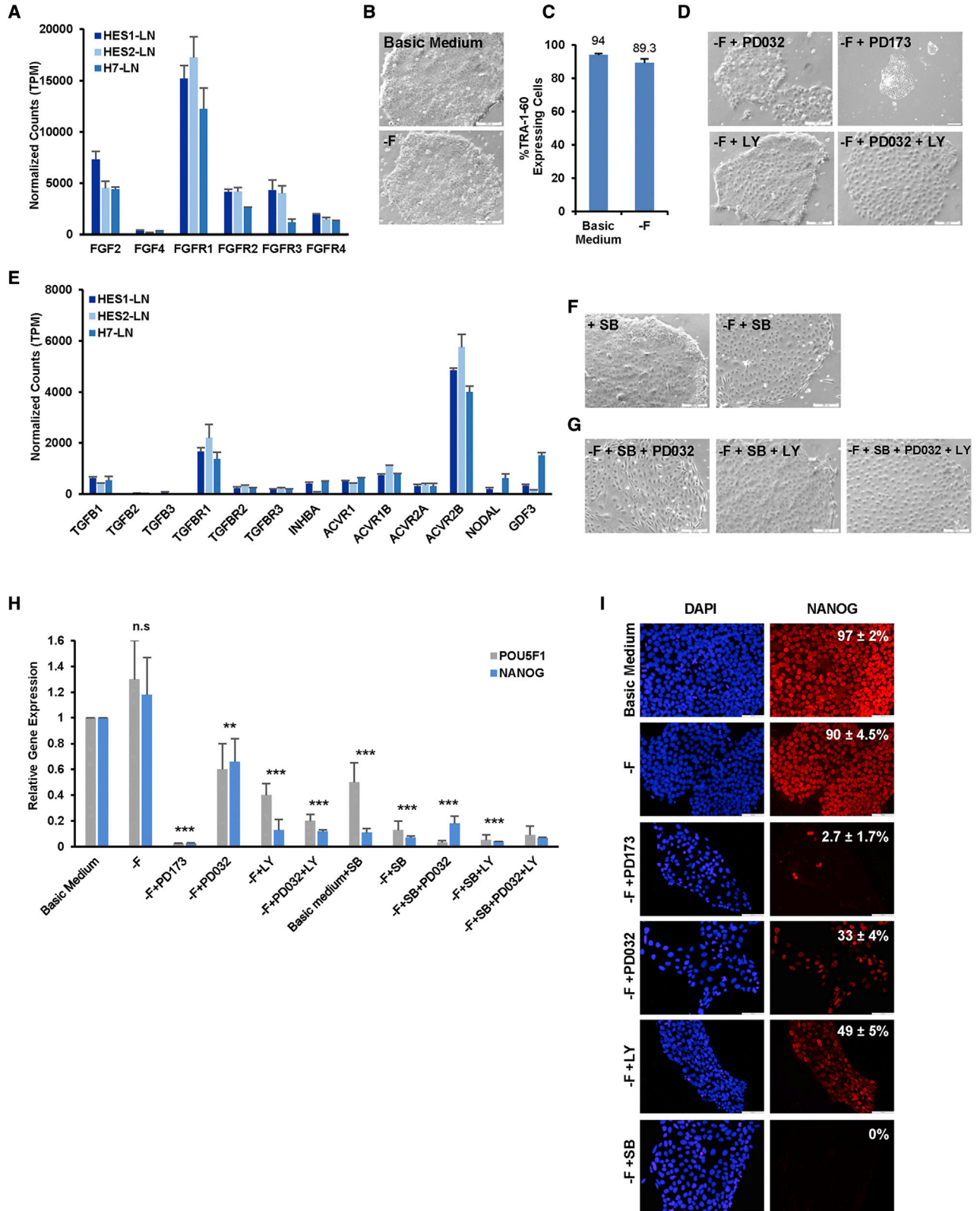
(B) Unsupervised hierarchical clustering of RRBS data of LN, primed, and naive hPSCs.

(C) Heatmaps of the methylation levels of DMRs that were hypermethylated (left panel), or hypomethylated (right panel), in LN compared with primed hPSCs.

(D) Top 20 enriched pathways related to hypermethylated DMRs in LN compared with primed hPSCs. Analysis was performed using Metascape (Zhou et al., 2019b).

(E and F) Methylation profiles (E) and RNA-seq data (F) of selected genes in LN compared with primed hPSCs. RNA-seq data are mean \pm SEM of two independent samples (except for HES-1-LN, three samples).

LN, LN-hPSCs; P, primed hPSCs; N, naive hPSCs. p values were calculated using two-tailed Student's t test when two groups were compared, and ANOVA test when three groups were compared. * $p < 0.05$, ** $p < 0.01$, *** $p < 0.001$.



(legend on next page)



cultured in the basic medium (Figures 4C, 4H, and 4I). We further blocked the MEK/ERK and PI3K/AKT pathways by culturing the cells in a medium depleted of FGF2, in the presence of PD173074 (PD173), a FGFR1 inhibitor, PD0325901 (PD032), a specific MEK inhibitor, LY294002 (LY), a specific PI3K inhibitor, or both PD032 and LY. Differentiation was observed in all these conditions, as evidenced by changes in cell morphology (Figure 4D), and significant downregulation of POU5F1 and NANOG expression levels (Figures 4H and 4I).

We next analyzed the role of TGF- β signaling in promoting the undifferentiated state of LN-hPSCs. RNA-seq analysis showed that LN-hPSCs expressed *TGFB1* and *INHBA* (encoding activin A). TGF- β receptor type 1 (*TGFBRI*) and activin A receptor type 2B (*ACVR2B*) were expressed at higher levels compared with the other receptors (Figure 4E). LN-hPSCs, cultured for 5 days in the basic medium in the presence of SB431542 (SB), a selective inhibitor of TGF- β , and activin receptors, appeared partially differentiated (Figure 4F). Under these conditions, POU5F1 levels were moderately downregulated, while NANOG expression, reported to be a direct target of SMAD2/3 signaling in hPSCs (Xu et al., 2008), was drastically reduced (Figure 4H). Following FGF2 depletion, LN-hPSCs differentiated (Figure 4F), and POU5F1 and NANOG expression levels were strongly reduced (Figures 4H and 4I). Upon culturing of LN-hPSCs without FGF2 supplementation, and with various combinations of SB, PD032, and LY, small numbers of colonies with a differentiated morphology survived (Figure 4G), and POU5F1 and NANOG levels decreased significantly (Figure 4H).

We analyzed the role of FGF- and TGF- β -dependent signaling in LN-hPSCs compared with primed, and naive hPSCs. Primed hPSCs showed similar dependency on FGF- and TGF- β signaling as LN-hPSCs (Figure S3A). In contrast, naive hPSCs remained undifferentiated in the presence of PD173 or SB but exhibited morphology changes and reduced NANOG expression when LY was added (Figure S3B). RNA-seq analyses showed similar expression levels of the various components of the FGF

and TGF- β signaling pathways in LN- and primed hPSCs that differed from naive hPSCs. Interestingly, the expression levels of *NODAL* were significantly lower in LN- compared with naive- and primed hPSCs (Figures S3C–S3E). Western blot analysis revealed similar expression levels of *p*-ERK in LN-hPSCs compared with primed hPSCs (Figure S3F).

These results showed that MEK/ERK, PI3K/AKT, and SMAD2/3 signaling pathways are required for the undifferentiated self-renewal of LN-hPSCs. They further showed autocrine/paracrine effects of FGF and TGF- β /activin A signaling on the maintenance of undifferentiated LN-hPSCs.

The canonical Wnt signaling is inactive in LN-hPSCs and its induction upregulates PS markers

During mouse embryonic development, the canonical Wnt/ β -catenin signaling is active in the ICM (Xie et al., 2008), downregulated in the early post-implantation epiblast (Sumi et al., 2013; ten Berge et al., 2011), and reactivated at the late post-implantation phase to promote the formation of the PS (Tam et al., 2006).

Assessment of the canonical Wnt signaling activity in LN-hPSCs (at passages 6–13) showed staining for β -catenin at the cell membranes, suggestive of inactive canonical Wnt signaling (Figures 5A and S4A–S4C). RNA-seq analysis of the expression of various components of the Wnt signaling in LN-hPSCs revealed relatively low expression levels (<100 TPM) of most ligands compared with other components of the Wnt signaling. Frizzled receptors *FZD5* and *FZD7* were expressed at higher levels (>3,700 TPM) compared with the other Frizzled receptors and *LRP5/6* co-receptors. *SFRP1* and *SFRP2*, antagonists of the Frizzled receptors, were expressed at higher levels (>6,800 TPM) compared with other antagonists (Figures 5B–5D). Consistent with a lack of canonical Wnt signaling, RNA-seq data showed minimal expression levels (<10 TPM) of the early PS markers *TBXT*, a target of Wnt signaling (Arnold et al., 2000), and *SOX17*, in LN-hPSCs (Figure 2F).

Figure 4. The FGF and TGF- β /activin dependent signaling pathways are required for the self-renewal of LN-hPSCs

(A and E) RNA-seq data of components of the FGF (A) and TGF- β /activin (E) signaling pathways in LN-hPSCs (HES-1, HES-2, and H7). Data are mean \pm SEM of two independent samples (except for HES-1-LN, three samples).

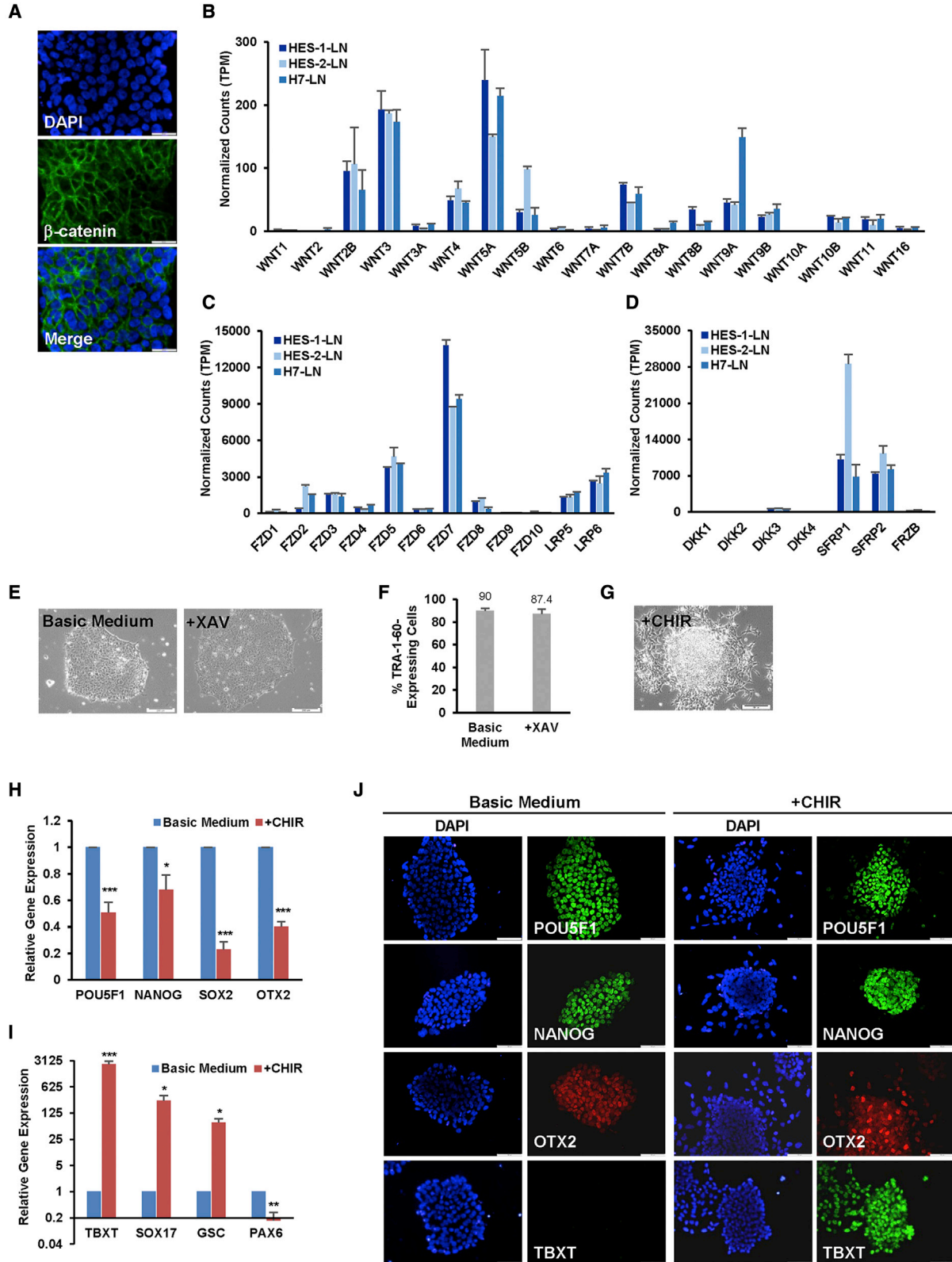
(B, D, F, and G) Phase-contrast images of HES-1-LN-hPSCs cultured in the basic medium containing FGF2, and in the absence of FGF2 (–F) (B), –F + PD173, –F + PD032, and –F + LY (D), SB, and –F + SB (F), and combinations of the various inhibitors (G). Scale bars, 200 μ m.

(C) FACS analysis of TRA-1-60 expression in HES-1-LN-hPSCs cultured \pm FGF2. Data are mean \pm SEM of three independent experiments.

(H) qRT-PCR analysis of the relative expression levels of POU5F1 and NANOG, in HES-1-LN-hPSCs cultured in the basic medium, and in the presence of the various inhibitors. Expression levels are normalized to the expression of β -actin. Data are mean \pm SEM of ($n \geq 3$) independent experiments except for –F + PD032 + LY, –F + SB + LY, –F + SB + PD032 + LY ($n = 2$).

(I) Immunostaining for NANOG (red) in HES-1-LN-hPSCs cultured in the presence of the various inhibitors. Nuclei are counterstained with DAPI (blue). Scale bars, 100 μ m.

Data are mean \pm SEM; n (fields) = 3 for all experiments. F, FGF2; PD032, PD0325901; PD173, PD17304; LY, LY294002; SB, SB431542. p values were calculated using two-tailed Student's t test for all samples compared with the basic medium sample. ** $p < 0.01$, *** $p < 0.001$.



(legend on next page)



Accordingly, immunostaining (at passages 3–13) did not detect TBXT- and SOX17-expressing cells in LN-hPSCs (Figures 5J, S4A–S4C, S4E, and S4F). Furthermore, culturing of LN-hPSCs in the presence of the Wnt signaling antagonist XAV939, did not affect their colony morphology or the percentages of cells expressing TRA-1-60 (Figures 5E and 5F). Taken together, these results suggested that LN111-based culture conditions promoted a relatively homogeneous population of hPSCs that uniformly exhibited inactive canonical Wnt signaling.

We further compared the expression of the various components of the canonical Wnt signaling pathways in LN-, primed, and naive hPSCs (Figures S4G–S4I). RNA-seq analysis revealed several components of Wnt signaling that were upregulated in LN- and primed hPSCs, compared with naive hPSCs, including *FZD7* and *SFRP1*. As shown above, *SFRP2* was expressed at significantly higher levels in LN- compared with primed hPSCs (Figure 2E), while *FZD5* expression was significantly lower in LN- compared with naive and primed hPSCs (Figures 3F and S4H).

In contrast to LN-hPSCs, immunostaining of primed hPSCs cultured in the basic medium showed a heterogeneous population expressing β -catenin at both the membrane and cytoplasm of cells. Moreover, primed hPSCs exhibited heterogeneous TBXT and SOX17 staining (Figures S4D–S4F). RNA-seq and qRT-PCR analyses further showed that primed hPSCs expressed higher levels of PS markers compared with LN-hPSCs (Figures 2F and S2G). These results suggested that, in contrast to LN-hPSCs, primed hPSCs exhibited heterogeneous canonical Wnt signaling activity.

To assess whether Wnt activation will promote LN-hPSC progression toward the PS stage, we cultured them for 3 days in the presence of FGF2 and CHIR99021 (CHIR), a canonical Wnt signaling agonist. Following treatment with CHIR, LN-hPSC colonies appeared differentiated with cells migrating from the colonies (Figure 5G), and β -catenin staining was observed in the cytoplasm

(Figures S4A–S4C). qRT-PCR showed a significant downregulation of the core pluripotency TFs as well as *OTX2*, concomitant with the upregulation of *TBXT*, *SOX17*, and *GSC*. The expression of the early neuroectodermal marker *PAX6* was not induced by CHIR (Figures 5H and 5I). Immunostaining for POU5F1, NANOG, and *OTX2* in the CHIR-treated LN-hPSCs showed reduced expression compared with control LN-hPSCs (Figure 5J). Immunostaining for TBXT and SOX17 showed upregulation of their expression upon Wnt activation (Figures 5J, S4A–S4C, S4E, and S4F). In contrast to LN-hPSCs, in CHIR-treated primed hPSCs the percentages of TBXT-expressing cells were not elevated, while the percentages of SOX17-expressing cells were augmented (Figures S4D–S4F).

Collectively, the suggested inactivity of the canonical Wnt signaling concomitant with the lack of PS marker expression in LN-hPSCs support their resemblance to early post-implantation epiblast. Their response to Wnt stimulation by induction of PS markers, suggest that they are poised for PS formation.

LN-hPSCs are competent to initiate germ cell specification

In the mouse embryo, the competence for PGC specification is restricted to the early post-implantation epiblast cells, and can be recapitulated *in vitro* by mEpiLCs (Hayashi et al., 2011; Ohinata et al., 2009). PGC competence was demonstrated for human PSCs exhibiting characteristics of naive-to-primed intermediate pluripotency states (Lau et al., 2020; Yu et al., 2021). Limited direct induction of PGC fate was also reported for primed hPSCs (Irie et al., 2015; Sasaki et al., 2015).

We explored the competence of LN-hPSCs to differentiate into PGCs in response to Wnt and BMP induction. These pathways were shown to be crucial for the induction of PGC specification in an evolutionarily conserved manner (Hayashi et al., 2011; Kobayashi et al., 2017; Ohinata et al., 2009).

Figure 5. The canonical Wnt signaling is inactive in LN-hPSCs, and its induction upregulates primitive streak markers

(A) Immunostaining for β -catenin (green) in HES-1-LN-hPSCs.

(B–D) RNA-seq data of various components of the canonical Wnt signaling in LN-hPSCs (HES-1, HES2, and H7). Data are mean \pm SEM of two independent samples (except for HES-1-LN, three samples).

(E) Phase-contrast images of HES-1-LN-hPSCs cultured in the basic medium, or in the presence of XAV939. Scale bars, 200 μ m.

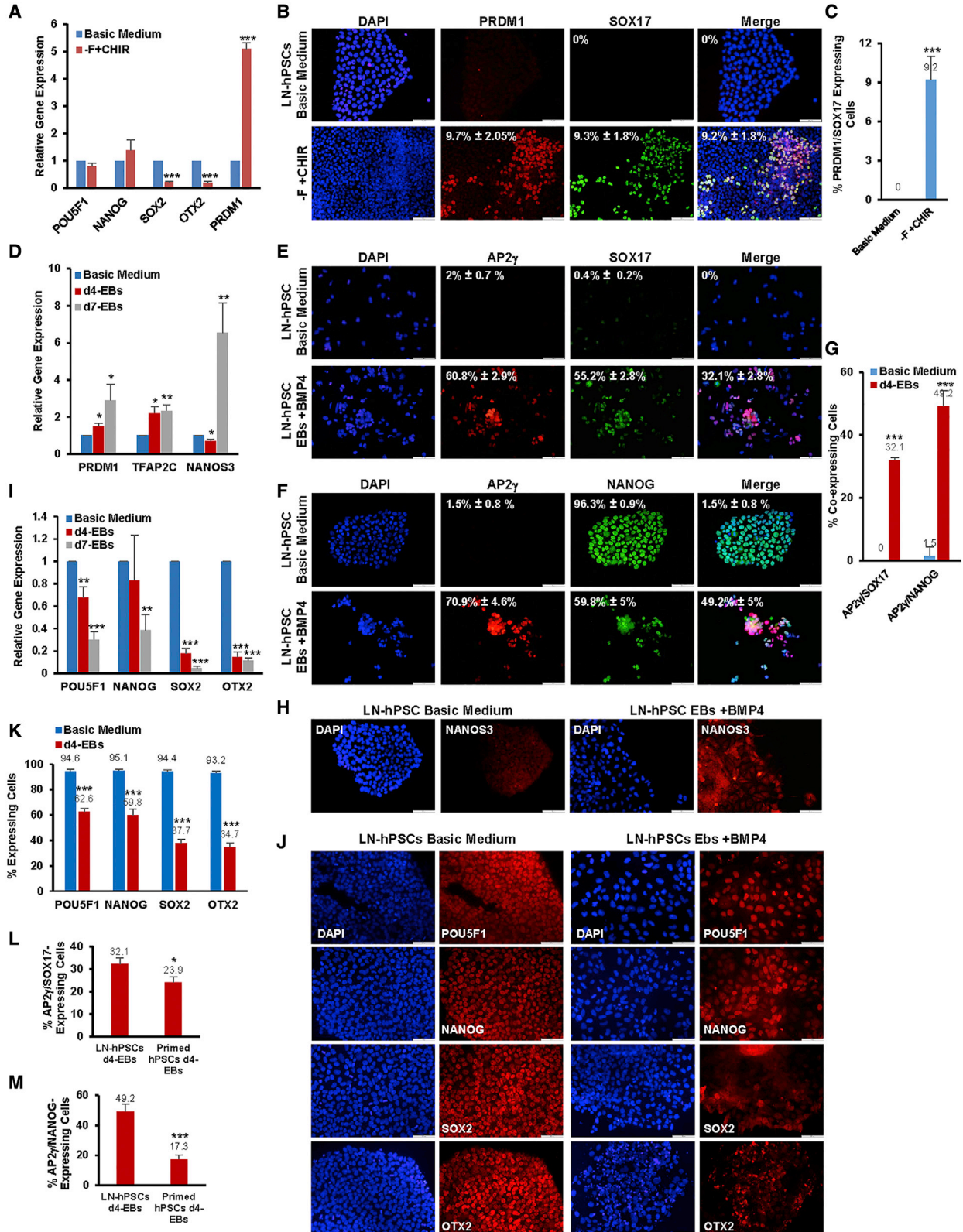
(F) FACS analysis of the expression of TRA-1-60 in HES-1-LN-hPSCs cultured as in (E). Data are mean \pm SEM of five independent experiments.

(G) Phase-contrast image of HES-1-LN-hPSCs cultured in the basic medium, in the presence of CHIR. Scale bar, 200 μ m.

(H and I) qRT-PCR analyses of the relative expression levels of pluripotency-associated markers (H), and lineage-specific markers (I), in HES-1-LN-hPSCs cultured in the basic medium, and in the presence of CHIR. Expression levels are normalized to the expression of GusB. Data are mean \pm SEM of (n) independent experiments; NANOG, TBXT (n = 5), POU5F1, SOX17, GSC, PAX6 (n = 4), SOX2, OTX2 (n = 3).

(J) Immunostaining for POU5F1, NANOG, OTX2, and TBXT in HES-1-LN-hPSCs cultured as in (H).

XAV, XAV939; CHIR, CHIR99021. p values were calculated using two-tailed Student's t test. *p < 0.05, **p < 0.01, ***p < 0.001. (A and J) Nuclei are counterstained with DAPI (blue). Scale bars, 100 μ m.



(legend on next page)



We first assessed the potential of the canonical Wnt signaling to initiate PGC specification. We cultured LN-hPSCs for 3 days in the basic medium without FGF2, in the presence of CHIR, and analyzed the expression of PRDM1 (BLIMP1) and SOX17, which were reported as early key regulators of human PGC specification (Irie et al., 2015). Following Wnt induction, qRT-PCR showed that the expression of PRDM1 was significantly upregulated (Figure 6A), and immunostaining showed a significant increase in cells co-expressing PRDM1 and SOX17 (Figures 6B and 6C). qRT-PCR further showed that, following Wnt induction, the expression levels of POU5F1 and NANOG were stable, while SOX2 and OTX2 levels decreased significantly (Figure 6A). Notably, human PGC-like cells (PGCLCs) were shown to express POU5F1 and NANOG, but not SOX2 (Chen et al., 2019). Moreover, in the mouse system, downregulation of *Otx2* preceded the initiation of PGC specification (Zhang et al., 2018).

We next analyzed the potential of BMP4 to induce PGC specification. LN-hPSCs (at passages 3–8) were cultured as embryoid bodies (EBs) for 7 days in the presence of BMP4, LIF, SCF, and EGF. qRT-PCR analysis of early PGC markers showed that the expression levels of PRDM1 and TFAP2C (encoding AP2 γ) were significantly upregulated already at day 4, while the expression of NANOS3 was significantly elevated at day 7 (Figure 6D). Early hPGCLCs were shown to co-express AP2 γ , SOX17, and NANOG (Chen et al., 2019; Zheng et al., 2019). We therefore analyzed their co-expression in day 4 BMP-induced EBs. Immunostaining of undifferentiated LN-hPSCs did not show cells co-expressing AP2 γ and SOX17, while only a minor fraction co-expressed AP2 γ and NANOG. Upon BMP4 induction, the percentages of AP2 γ ⁺SOX17⁺ and

AP2 γ ⁺NANOG⁺ cells increased significantly (Figures 6E–6G), as well as the expression of NANOS3 (Figure 6H). qRT-PCR analysis showed that the elevation of the expression of PGC markers was concomitant with a significant downregulation of the expression of POU5F1, NANOG, SOX2, and OTX2 (Figure 6I). Immunostaining analysis confirmed the significant decrease of cells expressing these TFs (Figures 6J and 6K). Notably, the downregulation of SOX2 and OTX2 expression was significantly more pronounced than POU5F1 and NANOG ($p < 0.001$).

We further compared the efficiency of PGC specification of LN-hPSCs with primed hPSCs. Immunostaining analysis of the co-expression of AP2 γ and SOX17, and AP2 γ and NANOG, in day 4 BMP4-induced EBs, showed significantly higher percentages of cells co-expressing these markers in EBs generated from LN-hPSCs compared with EBs generated from primed hPSCs (Figures 6L, 6M, and S5). These results suggested that LN-hPSCs could be directly induced by BMP4 to differentiate into PGCLCs at a significantly higher efficiency compared with primed hPSCs.

Collectively, our data suggested that LN-hPSCs are competent to initiate PGC specification.

DISCUSSION

Here, we show that, by recapitulating the main component of the embryonic ECM niche and defined culture conditions, we captured the early post-implantation pluripotent phase *in vitro*, establishing a highly enriched population of genetically stable, self-renewing hPSCs. These hPSCs can be propagated for multiple passages retaining their pluripotent potential, and exhibiting properties similar to mouse

Figure 6. LN-hPSCs are competent to initiate germ cell specification

(A) qRT-PCR analyses of the relative expression levels of pluripotency-associated markers and the early PGC marker PRDM1 in HES-1-LN-hPSCs cultured in the basic medium or in the basic medium without FGF2, and in the presence of CHIR. POU5F1 (n = 4), NANOG (n = 5), SOX2, OTX2, PRDM1 (n = 3).

(B and C) Immunostaining images (B) and quantification (C) for the expression of PRDM1 and SOX17 in HES-1-LN-hPSCs cultured as in (A). n = 3.

(D) qRT-PCR analyses of the relative expression levels of early PGC markers in HES-1-LN-hPSCs cultured in the basic medium, or as EBs, in the absence of FGF2, and in the presence of BMP4, LIF, SCF, and EGF. Basic medium, 4 days, BMP4-EBs (n = 4), 7 days, BMP4-EBs (n = 3).

(E–H) Immunostaining images (E and F) and quantification (G) for the co-expression of AP2 γ and SOX17 (E) and AP2 γ and NANOG (F), and Nanos3 expression (H), in HES-1-LN-hPSCs cultured as in (D). AP2 γ and SOX17, basic medium (n = 3); BMP4-EBs (n = 5); AP2 γ and NANOG, basic medium (n = 2), BMP4-EBs (n = 3).

(I) qRT-PCR analyses of the relative expression levels of POU5F1, NANOG, SOX2, and OTX2, in HES-1-LN-hPSCs cultured as in (D). Basic medium, 4 days-BMP4-EBs (n = 5), 7 days-BMP4-EBs (n = 3).

(J and K) Immunostaining images (J) and quantification (K) for the expression of POU5F1, NANOG, SOX2, and OTX2, in HES-1-LN-hPSCs cultured as in (D). n \geq 3.

(L and M) Quantification of immunostaining for the co-expression of AP2 γ and SOX17 (L), and AP2 γ and NANOG (M) in BMP4-induced EBs generated from HES-1-LN and primed hPSCs. n \geq 3.

F, FGF2; CHIR, CHIR99021; EBs, embryoid bodies. p values were calculated using two-tailed Student's t test. * $p < 0.05$, ** $p < 0.01$, *** $p < 0.001$. For all experiments, data are mean \pm SEM of (n) independent experiments. (A, D, and I) expression levels were normalized to the expression of GusB. (B, E, F, H, and I) Nuclei are counterstained with DAPI. Scale bars, 100 μ m.



and primate embryonic early post-implantation epiblasts, including competence to give rise to the germ cell lineage.

In the mouse embryo, a formative pluripotent phase was proposed to exist in the course of transition from the pre-implantation naive to the post-implantation primed epiblast (Pera and Rossant, 2021; Smith, 2017). Embryonic formative epiblast cells exhibit downregulation of naive, upregulation of post-implantation, and lack of expression of lineage-specific genes (Mohammed et al., 2017). PGC specification is restricted to the epiblast at the formative phase (Ohinata et al., 2009). The late post-implantation epiblast is more heterogeneous, expresses PS markers, and exhibits increased Wnt, BMP4, and FGF activities (Boroviak et al., 2015; Mohammed et al., 2017; Nakamura et al., 2016).

RNA-seq analysis of 3D cultures of human blastocysts showed that day 6–7 pre-implantation epiblast cells clustered separately from day 8–9 early post-implantation epiblast cells, indicating distinct pre- and early post-implantation epiblast transcriptomes (Xiang et al., 2020). In line with the mouse and human embryonic data above, our global transcriptome analyses showed that LN-hPSCs clustered distinctly from naive and primed hPSCs, although they were more closely related to primed hPSCs. Subtle differences in gene expression between formative-like hPSCs and primed hPSCs were previously observed (Kinoshita et al., 2021). Consistent with an early post-implantation gene expression profile, RNA-seq analyses showed that LN-hPSCs downregulated naive and upregulated early post-implantation epiblast markers. Notably, *SALL2* and *SFRP2*, which were upregulated in LN-hPSCs compared with naive and primed hPSCs, were shown to be upregulated in mouse, primate, and human early post-implantation epiblasts (Boroviak et al., 2015; Nakamura et al., 2016; Xiang et al., 2020), as well as during formative transition of naive hPSCs (Rostovskaya et al., 2019), suggesting the relevance of these markers to the human early post-implantation epiblast. Furthermore, LN-hPSCs showed minimal expression of early PS markers that were upregulated in primed hPSCs, as reported previously (Hough et al., 2014).

DNA methylation analysis of human embryos in 3D cultures showed a marked transition from the hypomethylated day 6 epiblast (26%) to the hypermethylated day 8 epiblast (50%), and day 10 epiblast (60%) (Zhou et al., 2019a). Consistent with the published data, our RRBS data showed that LN-hPSCs exhibited methylation levels that were distinct from the hypomethylated naive hPSCs and were comparable with primed hPSCs. Hypermethylated DMRs in LN- compared with primed hPSCs were enriched for pathways related to differentiation and morphogenesis, suggesting that these pathways may be downregulated in LN-hPSCs.

Mouse and primate early post-implantation epiblasts exhibit inactive canonical Wnt signaling (Mohammed et al., 2017; Nakamura et al., 2016; Sumi et al., 2013). Inhibition of Wnt signaling facilitates the transition of naive hPSCs to an early post-implantation phenotype (Kinoshita et al., 2021; Rostovskaya et al., 2019). Consistent with inactive Wnt signaling, LN-hPSCs displayed membranous β -catenin staining, expressed the Wnt antagonists *SFRP1* and *SFRP2*, and did not express early PS markers. In contrast, our data as well as others (Blauwkamp et al., 2012) showed that primed hPSCs exhibited heterogeneous Wnt signaling activity.

Germline specification was suggested as a criterion to define the human formative pluripotency state (Pera and Rossant, 2021). In accordance, naive-to-primed intermediate hPSCs could efficiently give rise to PGCLCs following BMP induction (Yu et al., 2021), while BMP induction of primed hPSCs resulted in low yields of PGCLCs (Irie et al., 2015; Sasaki et al., 2015). The limited capacity of primed hPSCs to differentiate into PGCLCs was argued to challenge the use of germline competence as a criterion to define formative hPSCs (Kinoshita et al., 2021). Nevertheless, it has been suggested to be attributed to the heterogeneity of primed hPSC cultures that may contain subpopulations with an earlier pluripotency state, or to the developmental plasticity of primed hPSCs (Pera and Rossant, 2021). Consistent with an early post-implantation epiblast identity, LN-hPSCs could directly respond to BMP induction, giving rise to early hPGCLCs at a significantly higher efficiency than primed hPSCs.

Our culture system is based on LN111 as the ECM protein, and a specific defined medium, both shown to play a role in the promotion of the early post-implantation epiblast state *in vivo* and *in vitro* (Hayashi et al., 2007, 2011; Li et al., 2003). Integrins are the major receptors mediating the attachment of hPSCs to various laminins, and their downstream signaling plays a role in mouse and human PSC self-renewal (Hayashi and Furue, 2016; Hayashi et al., 2007). Further studies are required to identify the specific integrins of LN-hPSCs, and the mechanism by which LN111-integrin signaling promotes the early post-implantation epiblast-like state. Additional studies may elucidate the relative contribution of the various components of our culture system to the pluripotency state of LN-hPSCs.

Our findings suggest that the LN111-based defined culture system promoted relatively homogeneous self-renewing hPSCs exhibiting properties of early post-implantation epiblasts. The relative homogeneous nature of LN-hPSC cultures was supported by the uniform expression of the core pluripotency TFs, as well as *OTX2* by the vast majority of LN-hPSCs. In addition, the canonical Wnt signaling was uniformly inactive, as indicated by the homogeneous β -catenin membranous staining, and lack of expression of

Table 1. The key properties of LN-hPSCs and recently reported hPSCs exhibiting characteristics of naive-to-primed intermediate pluripotency states

	Our study	Cornacchia et al. (2019)	Lau et al. (2020)	Kinoshita et al. (2021)	Yu et al. (2021)
Basal medium	N2/B27	E8	mTeSR or E8	N2/B27	N2/B27
Supplements	FGF2	FGF2, TGF- β	FGF2, TGF- β	activin A, XAV939, BMS493	FGF2, activin A, CHIR99021
Substrate	laminin-111 (~8 $\mu\text{g}/\text{cm}^2$)	vitronectin	Matrigel, or vitronectin	laminin and fibronectin	mouse embryonic fibroblast feeders, or Matrigel
Self-renewal	prolonged self-renewal of genetically stable hPSCs	high self-renewal	high self-renewal	prolonged self-renewal	prolonged self-renewal
Self-renewal signaling pathways	MEK/ERK, PI3K/AKT, SMAD2/3	decreased MAPK and TGF- β signaling	negative regulators of MAPK upregulated, components of NODAL signaling upregulated	not reported	not reported
Canonical Wnt signalling	inactive, poised to respond to Wnt induction	not reported	low expression of Wnt ligand and receptors, and expression of Wnt antagonist	inhibited by XAV939	induced by CHIR99021
Gene expression profile	low expression of naive markers (KLF2/4/17, DPPA2/3/5, TFCP2L1), expression of early post-implantation markers (SALL2, SFRP2, SOX11), no lineage priming	expression of general pluripotency and naive marker (KLF4)	low expression of the naive markers KLF17 and TBX3, and expression of the naive markers TFCP2L1 and DPPA2, expression of early post-implantation markers (POU3F1, OTX2), no lineage priming	low expression of the naive markers KLF4/17 and TFCP2L1, and expression of the naive markers DPPA2/3 and GDF3, expression of early post-implantation markers (OTX2, SOX11), no lineage priming	no expression of naive marker (KLF17), expression of early post-implantation marker (OTX2)
Methylation status	distinct from naive hPSCs, and resembling primed hPSCs and the post-implantation epiblast	slightly lower than primed hPSCs	similar to the total unfractionated population	not reported	not reported
Somatic lineages differentiation	tri-lineage differentiation <i>in vivo</i> and <i>in vitro</i> .	tri-lineage differentiation <i>in vivo</i> and <i>in vitro</i> , neural specification bias	tri-lineage differentiation <i>in vitro</i>	tri-lineage differentiation <i>in vitro</i>	tri-lineage differentiation <i>in vivo</i>
Germline specification	competence for germline specification	not reported	competence for germline specification	not reported	competence for germline specification
Additional characteristics	generated from conventional hPSCs, low cloning efficiency	high cloning efficiency	GCTM2/CD9/EPC-AM high subpopulation within hPSC cultures	generated from naive hPSCs, and pre-implantation embryos	reprogrammed from human fibroblasts, high cloning efficiency





TBXT, an early PS marker and target of the Wnt signaling, at the RNA and protein levels. Moreover, LN-hPSCs expressed minimal levels of additional early PS markers, such as SOX17. In contrast to LN-hPSCs, primed hPSCs were heterogeneous with regard to Wnt signaling activity and the expression of lineage-specific markers. The heterogeneity of primed hPSC cultures that may contain subpopulations with earlier pluripotency states (Hough et al., 2014) may enable their direct conversion to LN-hPSCs exhibiting an earlier pluripotency state.

Several recent studies reported on human PSCs exhibiting characteristics of naive-to-primed intermediate pluripotency states (Cornacchia et al., 2019; Kinoshita et al., 2021; Lau et al., 2020; Rostovskaya et al., 2019; Yu et al., 2021). The reported hPSCs differed in the culture conditions, supporting their self-renewal, the expression of pluripotency markers, and the activity of the canonical Wnt and MEK/ERK pathways (Table 1). LN-hPSCs, as well as most other reported naive-to-primed intermediate hPSCs, showed upregulated expression of early post-implantation epiblast markers, except for the hPSCs reported by Cornacchia et al., which exhibited naive protein expression, and inactive ERK signaling, suggesting that these hPSCs may represent an earlier developmental state. Inactive canonical Wnt signaling, which is a property of the early-post implantation mouse epiblast (Sumi et al., 2013), was observed in LN-hPSCs. Similar to LN-hPSCs, the hPSCs described by Kinoshita et al. exhibited inactive Wnt signaling; however, they were dependent on exogenous Wnt inhibition. In contrast, the hiPSCs reported by Yu et al. were dependent on activation of Wnt signaling, suggesting that they may represent an earlier intermediate state along the naive-to-primed transition. Finally, competence for PGC specification, which was suggested as a criterion to define human formative PSCs (Pera and Rossant, 2021), was shown for LN-hPSCs and two other reported intermediate hPSCs (Lau et al., 2020; Yu et al., 2021).

In summary, we show that hPSCs, with properties similar to the early post-implantation epiblast, can be stably propagated in culture. The formative-like nature and the relative homogeneity of hPSC cultures demonstrated here may be invaluable for studying human embryonic PSC development, and for induction of differentiation toward both somatic and germline lineages.

EXPERIMENTAL PROCEDURES

Resource availability

Corresponding author

Benjamin E. Reubinoff, BenR@hadassah.org.il

Materials availability

This study did not generate new unique reagents.

hPSC lines and culture under LN111-based conditions

hPSC lines used in this study were HES-1, HES-2 (Reubinoff et al., 2000), HAD-C100, HAD-C102 (Tannenbaum et al., 2012), and H7 (Thomson et al., 1998). LN-hPSCs were cultured on mouse LN111 (3D Culture Matrix Laminin I), in DMEM/F12 medium, containing N2/B27, and supplemented with FGF2.

Signaling pathway analysis

LN-hPSCs were cultured for 2 days in complete medium, and then for an additional 3–5 days in medium \pm FGF2, in the presence of PD173074, PD032590, LY294002, SB431542, CHIR99021, and XAV939.

RNA-seq library preparation, sequencing, and analysis

Total RNA was extracted from hPSCs, and mRNA libraries were prepared from 1 μ g RNA. Ten microliters of each library was collected and pooled. The multiplex sample pool was loaded onto the Illumina NextSeq 500 System, with 75 cycles and single-read sequencing conditions. Following quality control measures, filtered FASTQ files were mapped directly to transcriptome with Salmon v.1.4.0. Differential gene expression was explored with DESeq2. PCA, heatmaps, and clustering were performed with native R functions, ComplexHeatmap, dendextend, and custom R scripts.

BMP induction of PGC differentiation

hPSCs were dissociated into a single-cell suspensions, seeded into microwells of AggreWell400 24-well plates, and cultured in suspension for 4–7 days, in differentiation medium containing BMP4, hLIF, SCF, and EGF, as described elsewhere (Irie et al., 2015).

Detailed experimental procedures are provided in the [supplemental information](#).

DATA AND CODE AVAILABILITY

The accession number for RNA-seq., single-cell RNA-seq., and RRBS datasets reported in this paper is GEO: GSE206713

SUPPLEMENTAL INFORMATION

Supplemental information can be found online at <https://doi.org/10.1016/j.stemcr.2022.10.010>.

AUTHOR CONTRIBUTIONS

B.E.R. and M.G. conceived and designed the experiments, analyzed the data, and wrote the manuscript. M.G., I.W., Y.G., D.S., and T.T.T. performed the experiments. O.S. and T.F.M. performed the RRBS. Y.S. contributed to data analysis. S.E.R. designed the culture system.

ACKNOWLEDGMENTS

The study was supported by generous donations of Sidney and Judy Swartz, and Dan and Morrine Marantz, for the “Stem cells for women’s health initiative.” RNA-seq was performed by the Genomic Applications Laboratory, Faculty of Medicine, Hebrew University of Jerusalem, Israel.



CONFLICT OF INTERESTS

B.E.R. is a member of the journal's Editorial Board. He is a founder, holds shares, and is the Chief Scientific Officer of CellCure Neuroscience Ltd. The company did not fund the study presented in this manuscript and has no interest in its results. A patent application related to the data presented in this manuscript has been submitted.

Received: June 27, 2022

Revised: October 12, 2022

Accepted: October 13, 2022

Published: November 10, 2022

REFERENCES

- Arnold, S.J., Stappert, J., Bauer, A., Kispert, A., Herrmann, B.G., and Kemler, R. (2000). Brachyury is a target gene of the Wnt/beta-catenin signaling pathway. *Mech. Dev.* *91*, 249–258.
- Blauwkamp, T.A., Nigam, S., Ardehali, R., Weissman, I.L., and Nusse, R. (2012). Endogenous Wnt signalling in human embryonic stem cells generates an equilibrium of distinct lineage-specified progenitors. *Nat. Commun.* *3*, 1070.
- Boroviak, T., Loos, R., Lombard, P., Okahara, J., Behr, R., Sasaki, E., Nichols, J., Smith, A., and Bertone, P. (2015). Lineage-specific profiling delineates the emergence and progression of naive pluripotency in mammalian embryogenesis. *Dev. Cell* *35*, 366–382.
- Brons, I.G.M., Smithers, L.E., Trotter, M.W.B., Rugg-Gunn, P., Sun, B., Chuva de Sousa Lopes, S.M., Howlett, S.K., Clarkson, A., Ahrlund-Richter, L., Pedersen, R.A., et al. (2007). Derivation of pluripotent epiblast stem cells from mammalian embryos. *Nature* *448*, 191–195.
- Buecker, C., Srinivasan, R., Wu, Z., Calo, E., Acampora, D., Faial, T., Simeone, A., Tan, M., Swigut, T., and Wysocka, J. (2014). Reorganization of enhancer patterns in transition from naive to primed pluripotency. *Cell Stem Cell* *14*, 838–853.
- Chen, D., Sun, N., Hou, L., Kim, R., Faith, J., Aslanyan, M., Tao, Y., Zheng, Y., Fu, J., Liu, W., et al. (2019). Human primordial germ cells are specified from lineage-primed progenitors. *Cell Rep.* *29*, 4568–4582.e5.
- Cornacchia, D., Zhang, C., Zimmer, B., Chung, S.Y., Fan, Y., Soliman, M.A., Tchieu, J., Chambers, S.M., Shah, H., Paull, D., et al. (2019). Lipid deprivation induces a stable, naive-to-primed intermediate state of pluripotency in human PSCs. *Cell Stem Cell* *25*, 120–136.e10.
- Crossley, P.H., and Martin, G.R. (1995). The mouse *Fgf8* gene encodes a family of polypeptides and is expressed in regions that direct outgrowth and patterning in the developing embryo. *Development* *121*, 439–451.
- Evans, M.J., and Kaufman, M.H. (1981). Establishment in culture of pluripotential cells from mouse embryos. *Nature* *292*, 154–156.
- Gafni, O., Weinberger, L., Mansour, A.A., Manor, Y.S., Chomsky, E., Ben-Yosef, D., Kalma, Y., Viukov, S., Maza, I., Zviran, A., et al. (2013). Derivation of novel human ground state naive pluripotent stem cells. *Nature* *504*, 282–286.
- Gheldof, A., and Berx, G. (2013). Cadherins and epithelial-to-mesenchymal transition. *Prog. Mol. Biol. Transl. Sci.* *116*, 317–336.
- Hayashi, K., Ohta, H., Kurimoto, K., Aramaki, S., and Saitou, M. (2011). Reconstitution of the mouse germ cell specification pathway in culture by pluripotent stem cells. *Cell* *146*, 519–532.
- Hayashi, Y., and Furue, M.K. (2016). Biological effects of culture substrates on human pluripotent stem cells. *Stem Cells Int.* *2016*, 5380560.
- Hayashi, Y., Furue, M.K., Okamoto, T., Ohnuma, K., Myoishi, Y., Fukuhara, Y., Abe, T., Sato, J.D., Hata, R.I., and Asashima, M. (2007). Integrins regulate mouse embryonic stem cell self-renewal. *Stem Cell.* *25*, 3005–3015.
- Hough, S.R., Thornton, M., Mason, E., Mar, J.C., Wells, C.A., and Pera, M.F. (2014). Single-cell gene expression profiles define self-renewing, pluripotent, and lineage primed states of human pluripotent stem cells. *Stem Cell Rep.* *2*, 881–895.
- Irie, N., Weinberger, L., Tang, W.W.C., Kobayashi, T., Viukov, S., Manor, Y.S., Dietmann, S., Hanna, J.H., and Surani, M.A. (2015). SOX17 is a critical specifier of human primordial germ cell fate. *Cell* *160*, 253–268.
- James, D., Levine, A.J., Besser, D., and Hemmati-Brivanlou, A. (2005). TGFbeta/activin/nodal signaling is necessary for the maintenance of pluripotency in human embryonic stem cells. *Development* *132*, 1273–1282.
- Kinoshita, M., Barber, M., Mansfield, W., Cui, Y., Spindlow, D., Stirparo, G.G., Dietmann, S., Nichols, J., and Smith, A. (2021). Capture of mouse and human stem cells with features of formative pluripotency. *Cell Stem Cell* *28*, 453–471.e458.
- Kobayashi, T., Zhang, H., Tang, W.W.C., Irie, N., Withey, S., Klisch, D., Sybirna, A., Dietmann, S., Contreras, D.A., Webb, R., et al. (2017). Principles of early human development and germ cell program from conserved model systems. *Nature* *546*, 416–420.
- Lau, K.X., Mason, E.A., Kie, J., De Souza, D.P., Kloehn, J., Tull, D., McConville, M.J., Keniry, A., Beck, T., Blewitt, M.E., et al. (2020). Unique properties of a subset of human pluripotent stem cells with high capacity for self-renewal. *Nat. Commun.* *11*, 2420.
- Li, S., Edgar, D., Fässler, R., Wadsworth, W., and Yurchenco, P.D. (2003). The role of laminin in embryonic cell polarization and tissue organization. *Dev. Cell* *4*, 613–624.
- Miner, J.H., Li, C., Mudd, J.L., Go, G., and Sutherland, A.E. (2004). Compositional and structural requirements for laminin and basement membranes during mouse embryo implantation and gastrulation. *Development* *131*, 2247–2256.
- Mohammed, H., Hernando-Herraez, I., Savino, A., Scialdone, A., Macaulay, I., Mulas, C., Chandra, T., Voet, T., Dean, W., Nichols, J., et al. (2017). Single-cell landscape of transcriptional heterogeneity and cell fate decisions during mouse early gastrulation. *Cell Rep.* *20*, 1215–1228.
- Nakamura, T., Okamoto, I., Sasaki, K., Yabuta, Y., Iwatani, C., Tsuchiya, H., Seita, Y., Nakamura, S., Yamamoto, T., and Saitou, M. (2016). A developmental coordinate of pluripotency among mice, monkeys and humans. *Nature* *537*, 57–62.
- Nichols, J., and Smith, A. (2009). Naive and primed pluripotent states. *Cell Stem Cell* *4*, 487–492.



- Ohinata, Y., Ohta, H., Shigeta, M., Yamanaka, K., Wakayama, T., and Saitou, M. (2009). A signaling principle for the specification of the germ cell lineage in mice. *Cell* 137, 571–584.
- Pera, M.F., and Rossant, J. (2021). The exploration of pluripotency space: charting cell state transitions in peri-implantation development. *Cell Stem Cell* 28, 1896–1906.
- Petropoulos, S., Edsgård, D., Reinius, B., Deng, Q., Panula, S.P., Codeluppi, S., Plaza Reyes, A., Linnarsson, S., Sandberg, R., and Lanner, F. (2016). Single-cell RNA-seq reveals lineage and X chromosome dynamics in human preimplantation embryos. *Cell* 165, 1012–1026.
- Reubinoff, B.E., Pera, M.F., Fong, C.Y., Trounson, A., and Bongso, A. (2000). Embryonic stem cell lines from human blastocysts: somatic differentiation in vitro. *Nat. Biotechnol.* 18, 399–404.
- Rostovskaya, M., Stirparo, G.G., and Smith, A. (2019). Capacitation of human naive pluripotent stem cells for multi-lineage differentiation. *Development* 146. dev172916.
- Sasaki, K., Yokobayashi, S., Nakamura, T., Okamoto, I., Yabuta, Y., Kurimoto, K., Ohta, H., Moritoki, Y., Iwatani, C., Tsuchiya, H., et al. (2015). Robust in vitro induction of human germ cell fate from pluripotent stem cells. *Cell Stem Cell* 17, 178–194.
- Smith, A. (2017). Formative pluripotency: the executive phase in a developmental continuum. *Development* 144, 365–373.
- Stirparo, G.G., Boroviak, T., Guo, G., Nichols, J., Smith, A., and Bertone, P. (2018). Integrated analysis of single-cell embryo data yields a unified transcriptome signature for the human pre-implantation epiblast. *Development* 145. dev158501.
- Sumi, T., Oki, S., Kitajima, K., and Meno, C. (2013). Epiblast ground state is controlled by canonical Wnt/beta-catenin signaling in the postimplantation mouse embryo and epiblast stem cells. *PLoS One* 8, e63378.
- Tabibzadeh, S., and Hemmati-Brivanlou, A. (2006). Lefty at the crossroads of "stemness" and differentiative events. *Stem Cell*. 24, 1998–2006.
- Takashima, Y., Guo, G., Loos, R., Nichols, J., Ficiz, G., Krueger, F., Oxley, D., Santos, F., Clarke, J., Mansfield, W., et al. (2014). Resetting transcription factor control circuitry toward ground-state pluripotency in human. *Cell* 158, 1254–1269.
- Tam, P.P.L., Loebel, D.A.F., and Tanaka, S.S. (2006). Building the mouse gastrula: signals, asymmetry and lineages. *Curr. Opin. Genet. Dev.* 16, 419–425.
- Tannenbaum, S.E., Turetsky, T.T., Singer, O., Aizenman, E., Kirshberg, S., Ilouz, N., Gil, Y., Berman-Zaken, Y., Perlman, T.S., Geva, N., et al. (2012). Derivation of xeno-free and GMP-grade human embryonic stem cells—platforms for future clinical applications. *PLoS One* 7, e35325.
- ten Berge, D., Kurek, D., Blauwkamp, T., Koole, W., Maas, A., Eroglu, E., Siu, R.K., and Nusse, R. (2011). Embryonic stem cells require Wnt proteins to prevent differentiation to epiblast stem cells. *Nat. Cell Biol.* 13, 1070–1075.
- Tesar, P.J., Chenoweth, J.G., Brook, F.A., Davies, T.J., Evans, E.P., Mack, D.L., Gardner, R.L., and McKay, R.D.G. (2007). New cell lines from mouse epiblast share defining features with human embryonic stem cells. *Nature* 448, 196–199.
- Theunissen, T.W., Powell, B.E., Wang, H., Mitalipova, M., Faddah, D.A., Reddy, J., Fan, Z.P., Maetzel, D., Ganz, K., Shi, L., et al. (2014). Systematic identification of culture conditions for induction and maintenance of naive human pluripotency. *Cell Stem Cell* 15, 471–487.
- Thomson, J.A., Itskovitz-Eldor, J., Shapiro, S.S., Waknitz, M.A., Swiergiel, J.J., Marshall, V.S., and Jones, J.M. (1998). Embryonic stem cell lines derived from human blastocysts. *Science* 282, 1145–1147.
- Wang, X., Xiang, Y., Yu, Y., Wang, R., Zhang, Y., Xu, Q., Sun, H., Zhao, Z.A., Jiang, X., Lu, X., et al. (2021). Formative pluripotent stem cells show features of epiblast cells poised for gastrulation. *Cell Res.* 31, 526–541.
- Xiang, L., Yin, Y., Zheng, Y., Ma, Y., Li, Y., Zhao, Z., Guo, J., Ai, Z., Niu, Y., Duan, K., et al. (2020). A developmental landscape of 3D-cultured human pre-gastrulation embryos. *Nature* 577, 537–542.
- Xie, H., Tranguch, S., Jia, X., Zhang, H., Das, S.K., Dey, S.K., Kuo, C.J., and Wang, H. (2008). Inactivation of nuclear Wnt-beta-catenin signaling limits blastocyst competency for implantation. *Development* 135, 717–727.
- Xu, R.H., Peck, R.M., Li, D.S., Feng, X., Ludwig, T., and Thomson, J.A. (2005). Basic FGF and suppression of BMP signaling sustain undifferentiated proliferation of human ES cells. *Nat. Methods* 2, 185–190.
- Xu, R.H., Sampsell-Barron, T.L., Gu, F., Root, S., Peck, R.M., Pan, G., Yu, J., Antosiewicz-Bourget, J., Tian, S., Stewart, R., et al. (2008). NANOG is a direct target of TGFbeta/activin-mediated SMAD signaling in human ESCs. *Cell Stem Cell* 3, 196–206.
- Yu, L., Wei, Y., Sun, H.X., Mahdi, A.K., Pinzon Arteaga, C.A., Sakurai, M., Schmitz, D.A., Zheng, C., Ballard, E.D., Li, J., et al. (2021). Derivation of intermediate pluripotent stem cells amenable to primordial germ cell specification. *Cell Stem Cell* 28, 550–567.e12.
- Zhang, J., Zhang, M., Acampora, D., Vojtek, M., Yuan, D., Simeone, A., and Chambers, I. (2018). OTX2 restricts entry to the mouse germline. *Nature* 562, 595–599.
- Zheng, Y., Xue, X., Shao, Y., Wang, S., Esfahani, S.N., Li, Z., Muncie, J.M., Lkins, J.N., Weaver, V.M., Gumucio, D.L., et al. (2019). Controlled modelling of human epiblast and amnion development using stem cells. *Nature* 573, 421–425.
- Zhou, F., Wang, R., Yuan, P., Ren, Y., Mao, Y., Li, R., Lian, Y., Li, J., Wen, L., Yan, L., et al. (2019a). Reconstituting the transcriptome and DNA methylome landscapes of human implantation. *Nature* 572, 660–664.
- Zhou, Y., Zhou, B., Pache, L., Chang, M., Khodabakhshi, A.H., Tanaseichuk, O., Benner, C., and Chanda, S.K. (2019b). Metascape provides a biologist-oriented resource for the analysis of systems-level datasets. *Nat. Commun.* 10, 1523.